Microfabricated Surface-Electrode Ion Trap for Scalable Quantum Information Processing

S. Seidelin,* J. Chiaverini,† R. Reichle,‡ J. J. Bollinger, D. Leibfried, J. Britton, J. H. Wesenberg, R. B. Blakestad, R. J. Epstein, D. B. Hume, W. M. Itano, J. D. Jost, C. Langer, R. Ozeri, N. Shiga, and D. J. Wineland

Time and Frequency Division, NIST, Boulder, Colorado 80305, USA

(Received 9 February 2006; published 30 June 2006)

Individual laser-cooled $^{24}Mg^{+}$ ions are confined in a linear Paul trap with a novel geometry where gold electrodes are located in a single plane and the ions are trapped 40 μm above this plane. The relatively simple trap design and fabrication procedure are important for large-scale quantum information processing (QIP) using ions. Measured ion motional frequencies are compared to simulations. Measurements of ion recooling after cooling is temporarily suspended yield a heating rate of approximately 5 motional quanta per millisecond for a trap frequency of 2.83 MHz, sufficiently low to be useful for QIP.

DOI: 10.1103/PhysRevLett.96.253003 PACS numbers: 32.80.Pj, 03.67.−a

Recent interest in coherent quantum state control and methods to realize practical quantum information processing (QIP) has led to impressive developments in quantum processing using several different physical systems [1]. Single quantum bit (qubit) rotations, two-qubit gates, and simple quantum algorithms have been implemented. However, perhaps the most significant challenge for any possible physical implementation of a quantum processor is to devise methods that scale to very large numbers of quantum information carriers.

The system of trapped ions is an interesting candidate for QIP because the basic requirements [2] have been demonstrated in separate experiments [1], and several schemes for scaling this system to large numbers of qubits have been proposed [1,3–7]. One approach is based on a network of interconnected processing and memory zones where ion qubits are selectively shuttled between zones [3,6]. Within this approach, miniature linear trap arrays [8–11] and a three layer T-junction trap [10] have been demonstrated. Since the speed of most multi-ion qubit gates is proportional to the ions' motional frequencies and these frequencies are inversely proportional to the square of the trap dimensions, we would like to decrease the size of these dimensions. To do this robustly, microfabrication techniques are required. Three-dimensional traps have been demonstrated with boron-doped silicon [12] and monolithically fabricated gallium-arsenide electrodes [11]. A significant simplification in fabrication could be achieved if all trap electrodes reside on a single surface and the ions are trapped above this surface [13]. In this case, the trapping electric fields would be the analog of magnetic fields used in ''chip'' traps for neutral atoms (see [14] and references therein). Surface-electrode ion traps have the potential added benefit for scaling that microelectronics for electrode potential control can be fabricated below the plane of the electrodes [15].

Recently, macroscopic charged particles have been confined in a surface-electrode trap [16]. Storage of atomic ions, however, requires substantially different experimental parameters. In this Letter we report the first demonstration of stable confinement of atomic ions in a surface-electrode trap. The trap is constructed with standard and scalable microfabrication processes. We load $^{24}Mg^{+}$ into this trap, measure the motional frequencies of the ions, and find reasonable agreement with those determined from simulations. We also determine a motional heating rate of the ion(s) that is low enough to allow for high fidelity logic operations.

The standard linear radio-frequency (rf) Paul trap [17] consists of four parallel rods whose centers are located on the vertices of a square [Fig. 1(a)]. An rf potential is applied to two opposing rods with the other two (control electrode) rods held at rf ground. This configuration creates a nearly harmonic ponderomotive pseudopotential in the $\hat{x}$-$\hat{y}$ plane. Longitudinal confinement for a single trapping zone is obtained by segmenting the control electrodes along their length and applying appropriate static potentials to the different segments. Several variations on this design have been demonstrated [8–12], but it is very desirable to simplify their construction. A straightforward way to modify the 3D design of Fig. 1(a) is to place the four rods in a common plane, with alternating rf and control electrodes [13]; one version of this geometry is shown in Fig. 1(b). In this design, the rods are replaced with flat electrodes, as shown in Fig. 2.

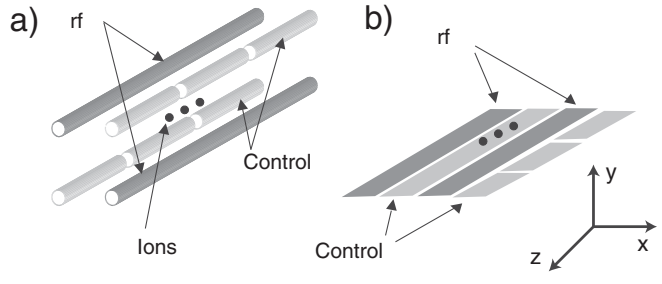

FIG. 1. (a) Standard linear rf Paul trap; (b) surface-electrode geometry where all electrodes reside in a single plane, with the ions trapped above this plane.

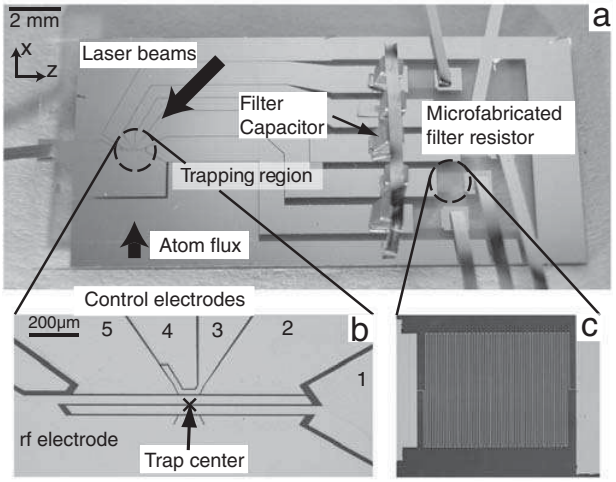

FIG. 2. Pictures of the surface-electrode trap. (a) The complete trap structure, including lead-out wires (ribbons) and filter capacitors. The directions of the laser beams (cooling and photoionization) and atom flux are indicated. (b) Expanded view of the trap region (center marked by ×). The control electrodes are numbered for reference in the text. (c) On-board meander line resistor.

We can fabricate this electrode structure by means of photolithography and metal deposition using evaporation and electrodeposition. For the substrate we use polished fused quartz, a material with low rf loss. A 0.030 μm titanium adhesion layer and a 0.100 μm copper seed layer are first evaporatively deposited onto the substrate. This deposition is uniform except for small areas for resistors where the quartz is left exposed. Resistors (~ 1 kΩ) and leads are fabricated through a liftoff process that entails patterning them with standard photolithography and evaporation of a 0.013 μm titanium adhesion layer followed by 0.300 μm of gold. Resistors are fabricated directly on the quartz substrate; leads are fabricated on top of the copper seed layer. The gold electrodes near the trapping region are electroplated onto the copper seed layer after a second photolithographic patterning step. Afterward, the exposed initial seed and adhesion layers are etched away to isolate electrodes and leads. The trap electrodes are plated to a thickness of ~ 6 μm so that the ratio of height to interelectrode spacing is relatively high (the interelectrode spacing is ~ 8 μm). This should reduce alteration of the trapping potential due to stray charges that may collect on the exposed insulator between electrodes.

We create ions in the trap by photoionizing thermally evaporated neutral magnesium atoms. The magnesium source is realized by resistively heating a stainless steel tube containing solid magnesium, which is sealed at both ends and has a small slit from which evaporated magnesium atoms emerge. With a planar electrode geometry, there is a risk of shorting electrodes to each other due to magnesium deposited onto the trap structure. To reduce this risk, in a last processing step we perform a controlled hydrofluoric acid (HF) etch of the central trap region. The HF etches away a small part of the titanium adhesion layer and the substrate, without affecting the electrodes. The result is an ~ 2 μm horizontal undercut of the electrodes to help prevent shorting due to deposition from the magnesium source. As a further precaution, we direct the magnesium flux nearly parallel to the surface and avoid as much as possible having the channels between electrodes be parallel to the flux (Fig. 2).

We use five independent control electrodes to provide sufficient degrees of freedom to be able to overlap the electric field null point of the static potential and the rf pseudopotential minimum. We create a low impedance path for the rf to ground on the control electrodes with capacitors (820 pF) that are surface mounted directly onto the chip (in the future, capacitors could be included as part of the fabrication process). Gold ribbons for applying the electrode potentials are gap welded to contact pads.

The trap structure is mounted in a copper tube that also serves as part of an rf transformer [18] and the entire structure is surrounded by a quartz envelope. The system is baked under vacuum prior to operation to reach a base pressure below 10^{-8} Pa with the use of an ion getter pump combined with a titanium sublimation pump.

As we describe below, the trap well depth U_T for a surface-electrode trap is fairly shallow [13], not much above the mean kinetic energy of the neutral atoms before they are ionized. Nevertheless, we can load $^{24}Mg^+$ ions efficiently by resonant two-photon photoionization (PI) at 285 nm [19]. The PI laser, resonant with the $3s^2\,{}^1S_0 \leftrightarrow 3s3p\,{}^1P_1$ electric dipole transition in neutral magnesium, copropagates with a Doppler-cooling beam tuned approximately 400 MHz below the $3s\,{}^2S_{1/2} \leftrightarrow 3p\,{}^2P_{1/2}$ electric dipole transition in $^{24}Mg^+$ at 280 nm. The laser beams are parallel to the trap surface, and at an angle of approximately 45° with respect to the trap $\hat{z}$ axis as shown in Fig. 2(a).

Since the laser beam direction has significant overlap with all principal trap axes, cooling will be efficient in all directions [13]. During loading, both the Doppler-cooling and PI beams have 2 mW power and waists of ~ 40 μm. The atomic flux of magnesium intersects the laser beams at the trap [Fig. 2(a)]. The cooling beam is applied continuously, while the PI beam needs to be applied for only a few seconds to create ions in the trap. Ions are loaded with the first configuration of trap potentials of Table I, which has the largest trap depth. Ions are detected by observing $3p\,{}^2P_{1/2} \leftrightarrow 3s\,{}^2S_{1/2}$ fluorescence along a direction perpendicular to the trap surface with a CCD camera as in the view of Fig. 2(b). Despite the fact that the center of the laser beam is only 40 μm above the surface, which increases the risk of scatter from light striking the trap electrodes, the signal-to-background ratio for scattered light from the ions is greater than 100 when the Doppler-cooling laser is tuned for minimum temperature, approxi-

mately 20 MHz (one-half linewidth) below resonance with intensity slightly below saturation.

We measure the oscillation frequencies of an ion in the trap by applying an oscillating field to a control electrode and observing a change in fluorescence rate when the frequency of the applied field is equal to one of the motional frequencies, thereby heating the ion [18]. To excite the axial (transverse) mode, we apply the oscillating field to electrode 2 (1).

As an aid in initially determining the correct operating conditions, trapping potentials are determined using numerical solvers (boundary element method) subject to the constraint that the rf pseudopotential minimum overlaps the null points of the electric field from the static potential, to minimize rf micromotion (see, for example, [20]). For the experiments described here, the static potentials on each control electrode, expressed as a fraction of the potential V_5 on electrode 5 [Fig. 2(b)], are $V_1 = 0.320$, $V_2 = 0.718$, $V_3 = 0.738$, and $V_4 = -0.898$.

The peak potential amplitude V_{rf} applied to the rf electrode (87 MHz) is difficult to measure directly. To determine it, we measure the three mode frequencies for three different experimental conditions shown in Table I and compare them to simulations. Inputs to the simulations are V_5, the measured electrode dimensions, and the ratio of the two rf powers applied to the trap (which can be accurately measured). A least squares fit, weighting all 9 frequencies equally, gives the values of V_{rf}. Since, under ideal circumstances, one set of conditions is sufficient to extract V_{rf}, an indication of the agreement between experiment and theory is given by the level of agreement between measured and predicted frequencies for all three cases (a few percent here). We believe the primary cause for the disagreement is due to the presence of additional stray static potentials on the electrodes. Finally, we numerically determine U_T in the pseudopotential approximation [21,22] for the three cases of Table I. A transverse cross section [the $\hat{x}$-$\hat{y}$ plane of Fig. 1(b)] of the trapping potential for $V_5 = 5$ V and $V_{\mathrm{rf}} = 103.2$ V near the central trap region is shown in Fig. 3.

TABLE I. Oscillation frequencies [experimental measurements (Expt.) and simulated values (Sim.)] for three different potential configurations explained in the text. The axial frequency is denoted $f_\parallel$, while $f_{\perp 1}$ and $f_{\perp 2}$ are the frequencies of the two transverse modes whose axes are indicated by the cross in Fig. 3. The uncertainties in the experimental values for the frequencies are approximately 0.10 MHz.

V_5 (V)	V_{rf} (V)	$f_\parallel$ (MHz)	$f_{\perp 1}$ (MHz)	$f_{\perp 2}$ (MHz)	U_T (meV)	
5.00	103.2(5)	2.83	15.78	17.13		(Expt.)
		2.77	15.62	17.17	177(6)	(Sim.)
2.00	103.2(5)	1.84	15.87	16.93		(Expt.)
		1.75	16.18	16.78	193(11)	(Sim.)
5.00	46.1(2)	2.85	5.28	8.29		(Expt.)
		2.77	5.02	8.73	6(1)	(Sim.)

In Fig. 4, we show groups of ions for the $V_{\mathrm{rf}} = 103.2$ V and $V_5 = 2.00$ V configuration. The separation of the ions is related to the center-of-mass axial oscillation frequency [3], and the horizontal bars indicate the expected ion separations according to the measurement of this frequency. When the number of ions becomes large enough, the string breaks into a zigzag configuration (see, for example, [23]).

Because $^{24}Mg^+$ lacks hyperfine structure, we cannot easily determine ion motional heating rates near the quantum limit using Raman transitions [24] (without applying large magnetic fields) due to poor internal state discrimination. An approximate value can be determined as follows. After nulling rf micromotion [20], we adjust the cooling beam for minimum temperature (see above). The beam is then blocked for a period to allow the ion to heat up. Upon resuming cooling, the fluorescence is initially smaller than its steady state value due to Doppler broadening; as the ion recools, the Doppler broadening lessens and the fluorescence increases until it reaches its steady state value given by the Doppler-cooling limit. We examine this recooling data for conditions where $\{f_\parallel, f_{\perp 1}, f_{\perp 2}\} = \{2.83, 15.78, 17.13\}$ MHz (Table I). Since heating (dE/dt) is observed to be stronger at lower frequencies [25,26], we will assume that the axial direction is predominantly heated. We detect fluorescence in successive time bins of 50 μs duration and find that the initial averaged fluorescence decreases after blocking the cooling beam a few seconds. We compare these results to simulations where we assume the ion (after the beam-blocked period) under-

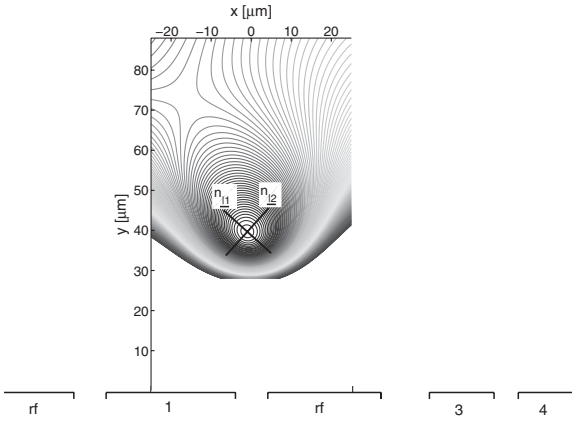

FIG. 3. A transverse cross section of the simulated trapping potential (both rf pseudopotential and static potentials included) for potentials corresponding to $V_5 = 5.00$ V and $V_{\mathrm{rf}} = 103.2$ V ($U_T = 177$ meV). The cross indicates the directions of the normal mode axes $\mathrm{n}_{\perp 1}$ and $\mathrm{n}_{\perp 2}$, and the expected position for an ion at the center of the trap in the $\hat{x}$-$\hat{y}$ plane. The separation between contour lines corresponds to 5 meV. The electrodes are depicted to scale in the lower part of the figure and labeled as in Fig. 2(b).

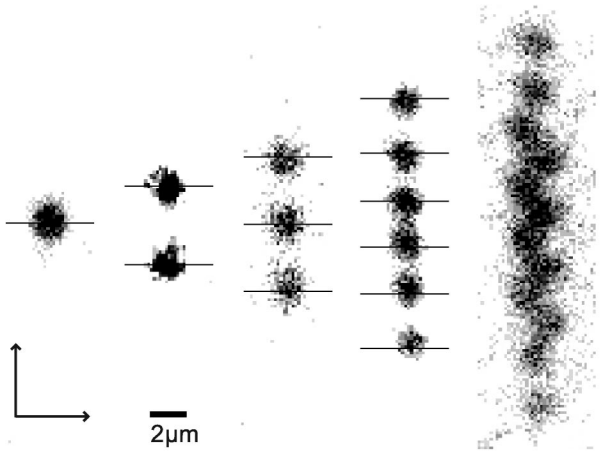

FIG. 4. Images of 1, 2, 3, 6, and 12 ions confined in the surface-electrode trap ($V_{\mathrm{rf}} = 103.2$ V and $V_5 = 2.00$ V). The length scale is determined from a separate image of the electrodes whose dimensions are known. The horizontal bars indicate the separation distance between the ions as predicted from the measured axial oscillation frequency. The ratio between transverse and axial oscillation frequencies makes it energetically favorable for the 12 ion string to break into a zigzag shape (see, for example, [23]).

goes harmonic oscillations with an amplitude corresponding to the Maxwell-Boltzmann energy distribution. Cooling is assumed to proceed as described in [27], which then determines fluorescence versus time. Comparing experiments and simulations for blocking times between 1 and 10 s, we determine an axial heating rate of 4.8 ± 0.4 quanta per millisecond (statistical uncertainty). This heating rate should be sufficiently small to allow high fidelity QIP operations [28].

The heating determined this way includes the effects of ion or neutral collisions and should give an upper limit on the heating that affects QIP [29]. Also, the heating rate determined here agrees with that determined from the escape time from the shallow well ($U_T \simeq 6$ meV). In [11], this method gave a significantly higher value than that determined using Raman transitions.

Johnson noise in the resistance of the *RC* filters on the control electrodes is a potential source of heating [3], but we theoretically estimate it to contribute only 1 quantum per second. Therefore the observed heating is apparently dominated by anomalous heating as observed in other experiments [25,26]. We note that in the presence of Doppler-cooling light, the lifetime of the ion is several hours (in the trap with $U_T = 177$ meV), presumably limited by chemical reactions [30].

An important next step is to replace $^{24}Mg^+$ with, for example, $^{25}Mg^+$ or $^{9}Be^+$, to study heating at the quantum level [24,25]. A longer-term goal is to design and fabricate a 2D array of surface-electrode trapping zones [6].

We thank E. Langlois and J. Moreland for advice on the microfabrication processes and Y. Le Coq for helpful comments on the manuscript. This work was supported by the Advanced Research and Development Activity (ARDA) under Contract No. MOD-7171.05 and NIST. S. S. wishes to thank the Carlsberg Foundation for financial support. Likewise, J. H. W. thanks the Danish Research Agency.

Note added in proofs.—After submission of this manuscript, trapping of strontium ions in a surface-electrode trap has also been reported [31].

*Electronic address: seidelin@boulder.nist.gov
†Present address: Los Alamos National Laboratory, Los Alamos, NM 87545, USA.
‡Present address: Quantum Information Processing, University of Ulm, D-89069 Ulm, Germany.

[1] See, for instance, http://qist.lanl.gov/qcomp_map.shtml.
[2] D. P. DiVincenzo, Fortschr. Phys. **48**, 771 (2000).
[3] D. J. Wineland *et al.*, J. Res. Natl. Inst. Stand. Technol. **103**, 259 (1998).
[4] R. G. DeVoe, Phys. Rev. A **58**, 910 (1998).
[5] J. I. Cirac and P. Zoller, Nature (London) **404**, 579 (2000).
[6] D. Kielpinski, C. Monroe, and D. J. Wineland, Nature (London) **417**, 709 (2002).
[7] L.-M. Duan *et al.*, Quantum Inf. Comput. **4**, 165 (2004).
[8] M. A. Rowe *et al.*, Quantum Inf. Comput. **2**, 257 (2002).
[9] M. D. Barrett *et al.*, Nature (London) **429**, 737 (2004).
[10] W. K. Hensinger *et al.*, Appl. Phys. Lett. **88**, 034101 (2006).
[11] D. Stick *et al.*, Nature Phys. **2**, 36 (2006).
[12] D. J. Wineland *et al.*, in *Proceedings of the XVII International Conference on Laser Spectroscopy, Avemore, Scotland, 2005*, edited by E. A. Hinds, A. Ferguson, and E. Riis (World Scientific, Singapore, 2005), pp. 393–402.
[13] J. Chiaverini *et al.*, Quantum Inf. Comput. **5**, 419 (2005).
[14] R. Folman *et al.*, Adv. At. Mol. Opt. Phys. **48**, 263 (2002).
[15] J. Kim *et al.*, Quantum Inf. Comput. **5**, 515 (2005).
[16] C. E. Pearson *et al.*, Phys. Rev. A **73**, 032307 (2006).
[17] W. Paul, Rev. Mod. Phys. **62**, 531 (1990).
[18] S. R. Jefferts *et al.*, Phys. Rev. A **51**, 3112 (1995).
[19] D. N. Madsen *et al.*, J. Phys. B **33**, 4981 (2000).
[20] D. J. Berkeland *et al.*, J. Appl. Phys. **83**, 5025 (1998).
[21] H. G. Dehmelt, Adv. At. Mol. Opt. Phys. **3**, 53 (1967).
[22] P. K. Ghosh, *Ion Traps* (Clarendon Press, Oxford, 1995).
[23] Daniel H. E. Dubin, Phys. Rev. Lett. **71**, 2753 (1993).
[24] C. Monroe *et al.*, Phys. Rev. Lett. **75**, 4011 (1995).
[25] Q. A. Turchette *et al.*, Phys. Rev. A **61**, 063418 (2000).
[26] L. Deslauriers *et al.*, quant-ph/0602003.
[27] D. J. Wineland and W. M. Itano, Phys. Rev. A **20**, 1521 (1979).
[28] D. Leibfried *et al.*, Nature (London) **422**, 412 (2003).
[29] The duration of most QIP experiments ($\sim$1 ms) is small compared to the mean time between (coherence-destroying) collisions (typically $>$1 s). Hence collisions affect only a negligible fraction of the QIP experiments.
[30] K. Mølhave and M. Drewsen, Phys. Rev. A **62**, 011401 (2000).
[31] K. R. Brown *et al.*, quant-ph/0603142.